Eur. Phys. J. C (2023) 83:430
https://doi.org/10.1140/epjc/s10052-023-11599-4

THE EUROPEAN PHYSICAL JOURNAL C

Regular Article - Theoretical Physics

Production of strangeonium $\phi(1680)$ state in electromagnetic probe-driven scatterings and hadron–hadron ultraperipheral collisions

Chen Dong[1], Yuhang Hou[1], Xiao-Yun Wang[1,2,a], Ya-Ping Xie[3,4], Xurong Chen[3,4,5], Li Zhang[1]

[1] Department of Physics, Lanzhou University of Technology, Lanzhou 730050, China
[2] Lanzhou Center for Theoretical Physics, Key Laboratory of Theoretical Physics of Gansu Province, Lanzhou University, Lanzhou 730000, Gansu, China
[3] Institute of Modern Physics, Chinese Academy of Sciences, Lanzhou 730000, China
[4] University of Chinese Academy of Sciences, Beijing 100049, China
[5] Guangdong Provincial Key Laboratory of Nuclear Science, Institute of Quantum Matter, South China Normal University, Guangzhou 510006, China

Received: 17 March 2023 / Accepted: 8 May 2023
© The Author(s) 2023

Abstract In this work, the $\gamma p \to \phi(1680)p$ reaction is systematically studied based on the two gluon exchange model and the pomeron model. The calculation results show that the total cross section of $\phi(1680)$ photoproduction can reach more than 80 nb near the center-of-mass energy $W = 4$ GeV, so it is suggested that JLab and other experiments carry out relevant measurements. Moreover, under the framework of the vector meson dominance assumption, the scattering length of $\phi(1680)$ and proton interaction is estimated as 0.07 ± 0.01 fm from the cross sections predicted by the theoretical models, which is on the same order of magnitude as the $\phi(1020)$-p scattering length. In addition, the total cross section, number of events and rapidity distribution of $\phi(1680)$ production are predicted at Electron-Ion colliders (EICs) and ultra-peripheral collisions (UPCs) by using eSTARlight and STARlight code. The study of $\phi(1680)$ and relevant properties is of enlightening significance in better understanding the strangeonium family spectrum, and provides necessary data support for the future experiment of EICs and UPCs.

1 Introduction

The strangeonium ($s\bar{s}$) states are the focus of research because they are the bridge between light and heavy quarks [1], and can provide relevant non-perturbative QCD information [2] in the low-energy region where the effective theory of heavy quarks is not suitable. Under the framework of the relativistic quark model [3], the $s\bar{s}$ states are expected to have a spectroscopy similar to that of heavy quarkonia. And their decay is investigated in detail by the theoretical model $^3P_0$ of the decay of light mesons [4]. However, the current $s\bar{s}$ spectrum is somewhat deficient [2,5], and only a few experimentally measured vector mesons are broadly accepted as $s\bar{s}$ states: $\phi(1020)$, $\phi(1680)$, $h_1(1415)$, $f_2'(1525)$ and $\phi_3(1850)$. This is because the proportion of $s\bar{s}$ states produced among hadrons is small, and decay width exists, which leads to the poor results in strangeonium experiments.

In the particle data group (PDG), $\phi(1680)$, like $\phi(1020)$, is listed as a vector state with quantum number $I^G(J^{PC}) = 0^-(1^{--})$. The mass is suggested to be 1680 ± 20 MeV and the width is 150 ± 50 MeV. The evidence of $\phi(1680)$ was initially understood in $p\bar{p}$ annihilation experiment [6] and Kp experiment [7]. Then in 1971, the $m(\pi^+\pi^-\pi^0)$ spectrum analysis of $\pi^+ d \to pp\pi^+\pi^-\pi^0$ revealed the existence of a meson $\phi(1680)$ at 1.68 GeV mass region [8]. Further research was performed in 1981, the $\phi(1680)$ was first measured in the $e^+e^- \to K_S K^\pm \pi^\mp$ reaction [9] at the energy range 1.4–2.18 GeV, and the fitted mass (1.667 ± 0.012 GeV) and width (102 ± 36 GeV) can be well explained in the quark model. In subsequent analysis, the ratio of $\phi(1680)$ coupling to K^+K^- was found to be very small [10–12]. In addition, the various decay properties were predicted in Ref. [1], the decay of $\phi(1680)$ was found to be dominated by the $KK^*(892)$ mode in their calculations and predicted the partial width ratio,

$$\frac{\Gamma(KK)}{\Gamma(KK^*)} \approx 0.06, \tag{1}$$

[a] e-mail: xywang@lut.edu.cn (corresponding author)

Published online: 22 May 2023

which was close to 0.07 ± 0.01 measured by DMI [9]. At the same time, the ratio of $\Gamma(\eta\phi)$ and $\Gamma(KK^*)$ was predicted as,

$$R_{\eta\phi/KK^*} = \frac{\Gamma(\eta\phi)}{\Gamma(KK^*)} \approx 0.20, \tag{2}$$

agreeing with the result predicted in Refs. [4,13,14]. However, these results is about twice smaller than the 0.37 measured from the BaBar Collaboration [15]. Therefore, the ratio needs to be more accurately measured in future experiments. To clarify the relevant properties of $\phi(1680)$, we expect to observe the state from photoproduction experiments. The reaction of $\gamma p \to K^+K^-$ shows a clear mass structure with a mass of $M = 1753 \pm 3$ MeV/c^2 and a width of $\Gamma = 122 \pm 63$ MeV. And found that the difference in the mass may be due to interference from other mesons, but it does not rule out the possibility that the 1.75 GeV/c^2 is a new state [16]. However, although there has been much research on $\phi(1680)$ states, the study of $\gamma p \to \phi(1680)p$ channel is still relatively inadequate. Therefore, the photoproduction data must be systematically measured through experimental to study the physical properties of the $\phi(1680)$, especially in the $\gamma p \to \phi(1680)p$ channel.

The total cross section and differential cross section of $\gamma p \to \phi p$ at the near-threshold were predicted with the two gluon exchange model and the pomeron model [17], which were in good agreement with the experimental data. $\phi(1680)$ has the same structure as $\phi(1020)$, so it is reasonable to predict the cross section of $\gamma p \to \phi(1680)p$ with the identical models and parameters in this work. In addition, under the definition of the vector meson dominance assumption (VMD), the scattering length of $\phi(1680)$-p interaction at the-near threshold is studied as R changes. Here R is proportional to W, which is the ratio of the meson momentum $\mathbf{p_3}$ to the photon momentum $\mathbf{p_1}$.

Collisions between hadrons–hadrons are usually represented as ultraperipheral collisions (UPCs) [18–21]. When the impact parameter between the two nuclei is larger than the sum of the radii of the two nuclei, the strong interaction between the two nuclei is suppressed. But this effect cannot be ignored because the electromagnetic interaction is a long-range force. In addition, the electron–proton collisions in the Electron-ions collider (EIC) [22–25] will be an essential reaction in studying the nucleon structure. The major difference between an EICs and a UPCs is that the photons emitted by the electron beam of an EIC are very virtual. Therefore, EICs can be used to study the photoproduction in the large Q^2 range. The STARlight [26] and eSTARlight [27,28] are two existing and critical Monte Carlo algorithm programs. They can be used to study vector meson and exotic states production at EICs and UPCs [26,27]. At present, using these two programs can effectively study the XYZ state [29], the bottomonium-like Z_b [30], the charged final states $a_2^+(1320)$, and the hidden pentaquark state [31]. Therefore, in this work, the two programs are used to simulate the production of vector meson $\phi(1680)$. In order to exhibit more distinctly the variation in the relevant kinematics, we set up about 500,000 events and simulated the different consequences in the two Q^2 intervals. This will require higher luminosity EICs and UPCs to satisfy the requirements of future experiments.

A brief outline of the paper is organized as follows. The expression of the scattering length, the two gluon exchange and pomeron models are described in Sect. 2, along with a detailed discussion of vector meson production at EICs and UPCs. The cross section of $\phi(1680)$, scattering length of $\phi(1680)$-p and relevant results are presented in Sect. 3. A simple summary and discussion is given in Sect. 4.

2 Formalism

2.1 Scattering length

The absolute value of the scattering length reflects the coupling strength between the vector meson-proton (V–p) interaction. Under the definition of the vector meson dominance assumption (VMD), the relation between scattering length $|\alpha_{Vp}|$ and the differential cross section $d\sigma/dt$ of vector meson photoproduction is [32,33],

$$|\alpha_{Vp}| = \frac{|\mathbf{p}_3|\, g_V}{R\pi} \sqrt{\frac{1}{\alpha_{em}} \frac{d\sigma^{\gamma p \to Vp}}{dt}(W_{thr}, t_{thr})}, \tag{3}$$

with

$$|\mathbf{p}_1| = \frac{1}{2W}\sqrt{W^4 - 2\left(m_1^2 + m_2^2\right)W^2 + \left(m_1^2 - m_2^2\right)^2}$$
$$|\mathbf{p}_3| = \frac{1}{2W}\sqrt{W^4 - 2\left(m_3^2 + m_4^2\right)W^2 + \left(m_3^2 - m_4^2\right)^2} \tag{4}$$

where $R = |\mathbf{p}_3|/|\mathbf{p}_1|$ represents the ratio of meson momentum $|\mathbf{p}_3|$ to photon momentum $|\mathbf{p}_1|$ and g_v is the VMD coupling constant [34,35],

$$g_V = \sqrt{\frac{\pi\alpha_{em}^2 m_V}{3\Gamma_{e^+e^-}}}, \tag{5}$$

where m_V is the mass of $\phi(1680)$ meson and the lepton decay width $\Gamma_{e^+e^-}$ is estimated to be 0.42 keV [36]. In the model definition, the total cross section of vector meson photoproduction is obtained by integrating the differential cross section from t_{min} to t_{max},

$$\sigma^{\gamma p \to Vp} = \int_{t_{min}}^{t_{max}} \frac{d\sigma^{\gamma p \to Vp}}{dt} dt, \tag{6}$$

where $t_{min}(t_{max})$ is [37,38],

$$t_{min}(t_{max}) = \left(\frac{m_1^2 - m_3^2 - m_2^2 + m_4^2}{2W}\right)^2 - (p_{1cm} \mp p_{3cm})^2 \tag{7}$$

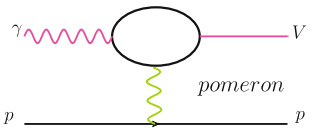

Fig. 1 The Feynman diagrams of the pomeron model for the vector mesons photoproduction

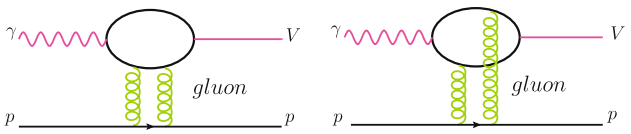

Fig. 2 The Feynman diagrams of the two gluon exchange model for vector mesons photoproduction

with $p_{icm} = \sqrt{E_{icm}^2 - m_i^2}$ $(i = 1, 3)$, $E_{1cm} = (W^2 + m_1^2 - m_2^2)/(2W)$ and $E_{3cm} = (W^2 + m_3^2 - m_4^2)/(2W)$.

When the centre of mass energy W approaches the threshold, $t_{min} \to t_{max}$, then the Eq. (6) becomes [33],

$$\sigma^{\gamma p \to Vp}(W_{thr}) = 4|\mathbf{p}_1||\mathbf{p}_3|\frac{d\sigma^{\gamma p \to Vp}}{dt}(W_{thr}, t_{thr}), \tag{8}$$

where the $4|\mathbf{p}_1||\mathbf{p}_3| = \Delta t = |t_{max} - t_{min}|$ and $t_{thr} = -m_V^2 m_p/(m_V + m_p)$. Then, by combining Eqs. (3) and (8), the $|\alpha_{Vp}|$ is calculated by the total cross section of vector meson photoproduction,

$$|\alpha_{Vp}| = \frac{g_V}{2\pi}\sqrt{\frac{\sigma^{\gamma p \to Vp}}{R\alpha_{em}}}, \tag{9}$$

where the α_{em} is the fine coupling constant

2.2 Pomeron model

The pomeron-quark interaction is flavour independence in the pomeron model [39], which provides a unique way to describe vector meson photoproduction. The fundamental interactions are described in Fig. 1. In the model, the differential cross section of vector meson is expressed as [39,40],

$$\frac{\mathrm{d}\sigma}{\mathrm{d}t} = \frac{81 m_V^3 \beta^4 \mu_0^4 \Gamma_{\mathrm{e^+e^-}}}{\pi \alpha_{em}} \left(\frac{s}{s_0}\right)^{2\alpha(t)-2} \times \left(\frac{F(t)}{\left(Q^2 + m_V^2 - t\right)\left(Q^2 + 2\mu_0^2 + m_V^2 - t\right)}\right)^2. \tag{10}$$

When $Q^2 = 0$, the formula represents the vector meson photoproduction, otherwise denotes vector meson electroproduction. The relevant coupling constant $\beta = 2$ GeV^{-1} and $\mu_0 = 1.1$ Gev^2. In Eq. (10), $\alpha(t) = 1.08 + 0.25t$ is the pomeron Regge trajectory [41], and $s_0 = 4$ GeV^2. $F(t)$ is the isoscalar form factor of the proton,

$$F(t) = \frac{4m_p^2 - 2.8t}{(4m_p^2 - t)(1 - t/0.7)^2} \tag{11}$$

where $m_p = 0.938$ GeV is the mass of proton.

2.3 Two gluon exchange model

The process of the two gluon exchange model is shown in Fig. 2. The photon is split into $q\bar{q}$, which scatters the initial proton through the exchange of two gluons and finally forms the vector meson. At the lowest order perturbation QCD, the differential cross section of vector meson photoproduction based on the two gluon exchange model is [40],

$$\frac{d\sigma}{dt} = \frac{\pi^3 \Gamma_{e^+e^-}\alpha_s}{6\alpha m_q^5}\left[xg\left(x, m_V^2\right)\right]^2 \exp\left(b_0 t\right). \tag{12}$$

Since the vector meson $\phi(1680)$ has the identical $s\bar{s}$ structure as $\phi(1020)$, the quark mass of the component is selected as $m_q = 0.486$ GeV, and the strong coupling constant α_s is set as 0.701. $xg(x, m_V^2)$ is the gluon distribution function, because the conventional gluon distribution functions such as the CTEQ6M [42], GRV98 [43], NNPDF [44] and CJ15 [45,46] cannot effectively interpret the photoproduction data of vector mesons at the near-threshold. Therefore, a parameterized gluon distribution function is introduced as $xg(x, m_V^2) = A_0 x^{A_1}(1 - x)^{A_2}$ [37,47]. The A_0, A_1, A_2, and the slope b_0 and are free parameters obtained by fitting experimental data. The total cross section is expressed by integrating Eq. (12) from t_{min} to t_{max},

$$\sigma(W) = \int_{t_{min}}^{t_{max}} \frac{d\sigma}{dt} dt. \tag{13}$$

2.4 The production of vector mesons at EICs and UPCs

For e–p scattering at EICs, the process of vector mesons production by exchanging virtual photons between hadrons and electrons is the vector meson electroproduction, which is closely connected to vector mesons photoproduction. The electroproduction cross section of mesons on a target proton is derived from Refs. [27,48],

$$\sigma(ep \to epV) = \int \frac{dW}{W}\int dk \int dQ^2 \frac{d^2 N_\gamma}{dk dQ^2}\sigma^{\gamma^* p \to Vp} \times \left(W, Q^2\right). \tag{14}$$

In the rest target frame, the momentum of the virtual photon emitted from the electron beam is denoted by k. W is the center of mass energy and $\sigma_{\gamma^* p \to Vp}(W, Q^2)$ is the cross

section of $\gamma^* p \to Vp$,

$$\sigma^{\gamma^* p\to Vp}\left(W, Q^2\right) = \sigma_{\gamma p\to Vp}\left(W, Q^2=0\right) \times \left(\frac{M_V^2}{M_V^2+Q^2}\right)^{\eta}, \quad (15)$$

where $\sigma^{\gamma p\to Vp}$ is the cross section of meson photoproduction. The $\eta = c_1 + c_2(Q^2 + m_V^2)$ is the variable which controls the flux, where $c_1 = 2.15 \pm 0.17$ and $c_2 = 0.0074 \pm 0.0046$ GeV^2 are two constants determined by HERA data [27]. The photo flux $d^2N_\gamma/dkdQ^2$ is given as [27,49],

$$\frac{d^2N_\gamma}{dkdQ^2} = \frac{\alpha}{\pi k Q^2}\left[1 - \frac{k}{Ee} + \frac{k^2}{2E_e^2} - \left(1-\frac{k}{Ee}\right)\left|\frac{Q^2_{\min}}{Q^2}\right|\right], \quad (16)$$

where $Q^2_{min} = m_e^2k^2/(E_e^2 - E_ek)$ with E_e represents the electron energy. The electron energy loss determines the maximum Q^2,

$$Q^2_{max} = 4E_e(E_e - k). \quad (17)$$

In the simulation of accelerator experiments, we can set the known electron beam energy E_e and photon virtuality Q^2 to calculate the total cross section of electron–proton (e–p) scattering at the near-threshold. In the laboratory frame, the ratio of photon energy K and $|t_{min}|$ is the rapidity of the final state [50],

$$y = \frac{1}{2}\ln\frac{k}{\sqrt{|t_{min}|}} = \ln\frac{2k}{m_V}. \quad (18)$$

In the target frame, the relationship between photon energy and rapidity is $k = 2\gamma_1 m_V/(2\exp(y))$, where the γ_1 represents the Lorentz boost of the ion. Here, the eSTARlight program is used to simulate the total cross-section electroproduction by e–p collision.

For UPCs, Eq. (14) can be rewritten as [26],

$$\sigma(pA \to pAV) = \int dk \frac{dN_\gamma(k)}{dk}\sigma^{\gamma p\to Vp}\left(W, Q^2\right), \quad (19)$$

where dN_γ/dk is similar to $d^2N_\gamma/dkdQ^2$ in the Eq. (14), representing the photon flux of ions [18] and A is heavy ion Au or Pb. Here, we exclusively consider the contribution of γp in the photon flux emitted by heavy ions. This is because the photon flux is directly proportional to the ion charge, and the photon flux of heavy ions is superior to that of protons [18,21]. We can simulate the production of vector mesons in proton and heavy ion reactions at the UPCs with STARlight [26].

3 Results

3.1 The reaction of $\gamma p \to \phi(1680)p$

In our previous work [17], the cross section of $\phi(1020)$ photoproduction was reproduced with the two gluon exchange model and the pomeron model, which was in good agreement with the experimental data. Relevant parameters for the two models are listed in Table 1. Through this set of parameters, the total cross section of $\phi(1680)$ photoproduction predicted by the two models are shown in Figs. 3 and 4 shows the differential cross section at the center of mass energy $W \in [2.62, 3.02]$ GeV, where $\Delta W = 0.08$ GeV. It can be observed that the cross sections of $\phi(1680)$ predicted by the two models are adjacent, and the cross section by the pomeron model is smaller than that based on the two gluon exchange model. As can be seen from Fig. 4, the two models exhibit different slopes. The differential cross section obtained by the pomeron model decreases faster with t than the two gluon exchange model, which is similar to the cross section of $\phi(1020)$ [17]. In addition, it can be found that the total cross section predicted by the theoretical model exceeds 80 nb at $W = 4$ GeV, which indicates that the JLab [51] and CLAS12 [52] laboratories can be carried out for relevant photoproduction experiments.

The variation of scattering length $|\alpha_{\phi(1680)p}|$ can be effectively observed from the differential cross section. With

Table 1 The relevant parameters for the two gluon exchange model and pomeron model

A_0	A_1	A_2	b_0 (GeV^{-2})	β (GeV^{-1})
0.36 ± 0.04	-0.055 ± 0.003	0.12 ± 0.03	3.60 ± 0.04	2.00

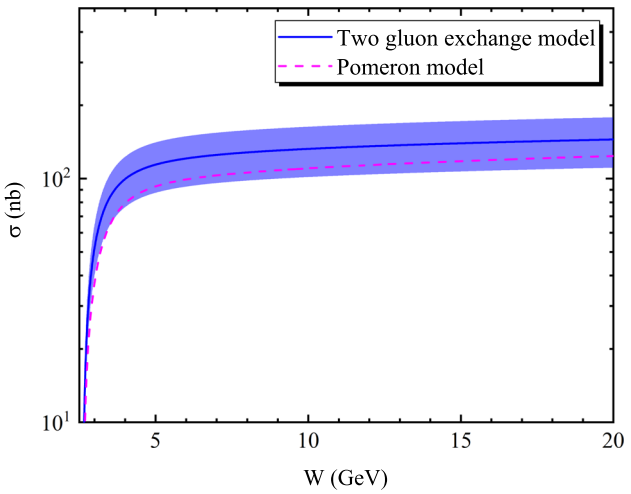

Fig. 3 The total cross sections of $\phi(1680)$ photoproduction predicted by the two gluon exchange model (the blue line) and the pomeron model (the magenta dashed-line)

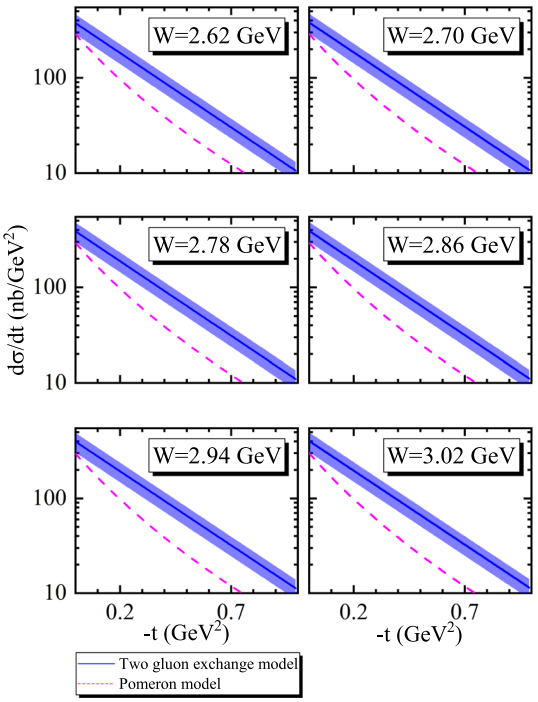

Fig. 4 The differential cross sections of $\phi(1680)$ photoproduction as a function of $-t$ at $W \in [2.62, 3.02]$ GeV, $\Delta W = 0.08$ GeV. Here, the notations are the same as in Fig. 3

Eq. (3), the $|\alpha_{\phi(1680)p}|$ as a function of R based on the differential cross sections predicted by the two models is shown in Fig. 5. Here, the R interval is chosen to be [0, 0.63]. The average scattering length is calculated as 0.075 ± 0.010 fm from the two gluon exchange model and 0.047 fm by the pomeron model. There exist some distinctions in consequences between the two models. The $|\alpha_{\phi(1680)p}|$ obtained based on the pomeron model is smaller than that based on the two gluon exchange model, which can be unambiguously understood from the behaviour of the differential cross section in Fig. 4. In addition, the slope of the differential cross section based on the pomeron is relatively large, resulting in $d\sigma/dt|_{t=t_{thr}}$ for the pomeron model being less than that for the two gluon exchange model.

Since the total cross section of $\phi(1680)$ predicted by the two models is adjacent at the near-threshold, the $|\alpha_{\phi(1680)p}|$ obtained does not differ significantly. As shown in Fig. 6, the $|\alpha_{\phi(1680)p}|$ based on the two models shows an upward trend with R, but the $|\alpha_{\phi(1680)p}|$ obtained from the two gluon exchange model is more prominent, the average scattering length is 0.084 ± 0.010 fm and 0.071 fm, corresponding to the two gluon exchange model and the pomeron model, respectively. Now, revisiting the $|\alpha_{\phi(1680)p}|$ obtained above, summarized in Table 2. The scattering length $|\alpha_{\phi(1680)p}|$ calculated based on the total cross section is larger than that derived by the differential cross section. In addition, the $|\alpha_{\phi(1680)p}|$ calculated by the total and differential cross section of the

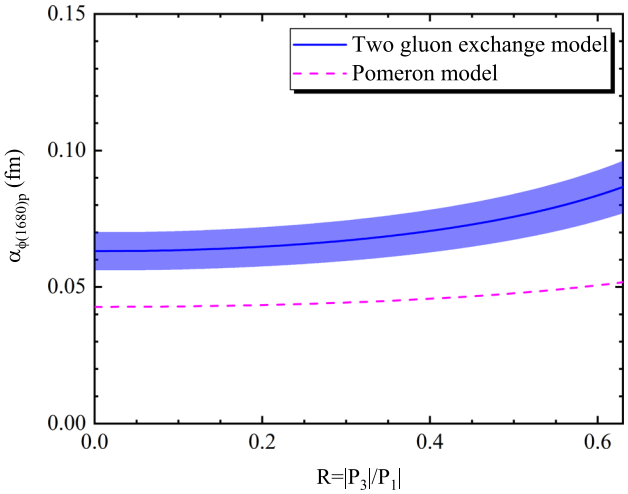

Fig. 5 The $|\alpha_{\phi(1680)p}|$ as function of R based on the differential cross sections. Here, the notations are the same as in Fig. 3

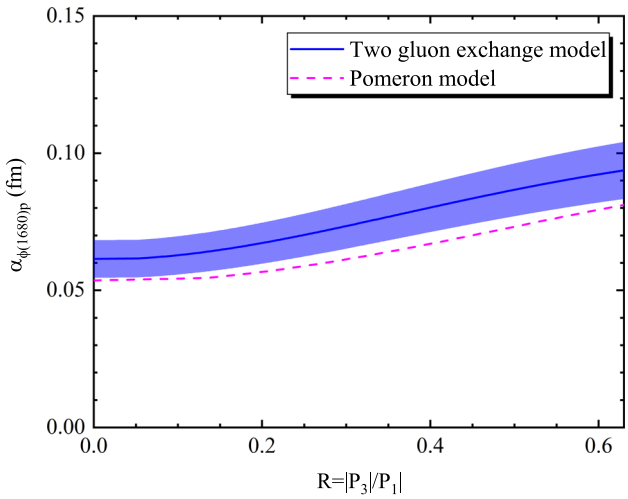

Fig. 6 The $|\alpha_{\phi(1680)p}|$ as function of R based on the total cross sections. Here, the notations are the same as in Fig. 3

two gluon model almost coincide with each other when considering the error. In contrast, the consequence derived by the pomeron model are quite different. Moreover, the result obtained by the two gluon exchange model are generally higher than those received by the pomeron model. However, we still require to consider all the results of the two models. This is because the free parameters of the pomeron model are small, which will cause small uncertainty factors. Therefore, considering all the results, the root mean square (RMS) is calculated as 0.07 ± 0.01 fm.

In our further discussion, one finds that the lepton decay width $\Gamma_{e^+e^-}$ does not affect the value of scattering length of $\phi(1680)$-p based on the two gluon exchange model and the pomeron model. This is because both models contain $\Gamma_{e^+e^-}$ and are located on the molecule. According to the relationship between the scattering length and the cross section estab-

Table 2 Scattering length of $\phi(1680)$-p estimated from the differential cross section $d\sigma/dt$ and total cross section σ based on the two gluon exchange model and pomeron data. The RMS is calculated as 0.07 ± 0.01 fm

Model	$\lvert\alpha_{\phi(1680)p}\rvert$ (fm)	
	$d\sigma/dt$	σ
Two gluon exchange model	0.075 ± 0.010	0.084 ± 0.010
Pomeron model	0.047	0.071

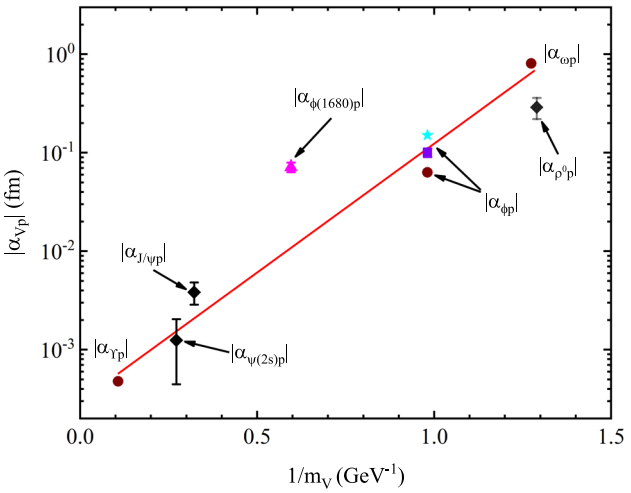

Fig. 7 The $|\alpha_{Vp}|$ as function of $\exp(1/m_V)$. The $|\alpha_{\phi(1680)p}| = 0.07 \pm 0.01$ fm of this work is represented by the magenta triangle. The black diamonds and purple square are from our previous work [53–55], the burgundy circle is from the work of Igor I. Strakovsky [35,56,57] and the cyan pentagram is from LEPS laboratory [58]

lished by the VMD model, $\Gamma_{e^+e^-}$ is just in the denominator, so the $\Gamma_{e^+e^-}$ cancel each other out in the calculation process. However, because lepton decay width is a critical factor in determining the specific size of the cross section of $\phi(1680)$ photoproduction based on the two models, it is necessary to measure $\Gamma_{e^+e^-}$ more accurately in future experiments.

Figure 7 shows the scattering lengths of different vector mesons $|\alpha_{Vp}|$ calculated with the VMD model. The $|\alpha_{\phi(1020)p}| = 0.10 \pm 0.01$ fm (the purple square) is taken from our previous work [53], which is very adjacent to the $|\alpha_{\phi(1680)p}|$ with a difference of only 0.03 fm. However, $|\alpha_{\phi(1680)p}|$ deviates from the main line, which is inconsistent with the scattering length of other vector mesons-proton interactions.

3.2 The prediction for $\phi(1680)$ production at EICs and UPCs

The rate of electroproduction is known to be a few percent of that of photoproduction, the first consideration is to use the eSTARlight code [27,28] to simulate e-p collisions at EICs. Table 3 displays the total cross section at four EICs at the

Table 3 The total cross sections of $ep \to ep\phi(1680)$ and event rates in e–p scattering at $0.10\ \text{GeV}^2 < Q^2 < 1.0\ \text{GeV}^2$ at eRHIC [22], EicC [23], JLEIC [24], LHeC [25]

Accelerator	eRHIC	EicC	JLEIC	LHeC
Energy e/p (GeV)	18/275	3.5/20	10/100	60/7000
σ (nb)	39	12	28	76
Event (B)	0.39	0.12	0.28	0.76

Table 4 The total cross sections of $ep \to ep\phi(1680)$ and event rates in e–p scattering at $1.0\ \text{GeV}^2 < Q^2 < 5.0\ \text{GeV}^2$ at eRHIC [22], EicC [23], JLEIC [24], LHeC [25]

Accelerator	eRHIC	EicC	JLEIC	LHeC
σ (nb)	10	3.0	7.0	20
Event (B)	0.10	0.03	0.07	0.20

$0.10\ \text{GeV}^2 < Q^2 < 1.00\ \text{GeV}^2$, and Table 4 lists the results at $1.00\ \text{GeV}^2 < Q^2 < 5.00\ \text{GeV}^2$. Obviously, the total cross section produced by high-energy EICs is larger than that produced by low-energy EICs, which means that the production of $\phi(1680)$ is more likely to be measured from high-energy facilities. In addition, in low-energy devices such as EicC [23], there are at least 300 million events, so the production of $\phi(1680)$ also has opportunity to be observed at low energy.

Figure 8 shows the rapidity distribution of $ep \to ep\phi(1680)$ in EICs obtained at $0.10\ \text{GeV}^2 < Q^2 < 1.00\ \text{GeV}^2$. And Fig. 9 illustrates the result at $1.00\ \text{GeV}^2 < Q^2 < 5.00\ \text{GeV}^2$. As expected, the higher the energy of the electron and proton beam emitted by the collider, the wider the rapidity distribution. This phenomenon is similar to the predicted change in the size trend of the total cross-section of $\phi(1680)$ electroproduction. Further, the eSTARlight code [27,28] is used to predict the mass distribution of $\phi(1680)$, as shown in the Fig. 10. And the variation interval and mass width can be witnessed. Here, only the result predicted at the EicC [23] is exhibited because the trends in the mass distribution produced by the different collider predictions almost overlap.

For a more detailed exploration of observations, we require a detector with appropriate capabilities in the experimental aspect of the forward region. For example, the pseudorapidity of the final meson is more widely distributed than its own photoproduction rapidity. And reggeon exchange is easier to explore EICs with moderate energy. So a high-energy collider like the LHeC would be difficult to achieve these goals. Therefore, this should be taken very carefully for $\phi(1680)$ and other vector mesons investigations.

For UPCs, the beam energies emitted and the calculation results are listed in Table 5 and Fig. 11 shows the rapidity distribution of $\phi(1680)$ predicted by the STARlight [26] program. For LHC [21] with high energy, the rapidity distribution is relatively wide. For RHIC [20], the rapidity distribu-

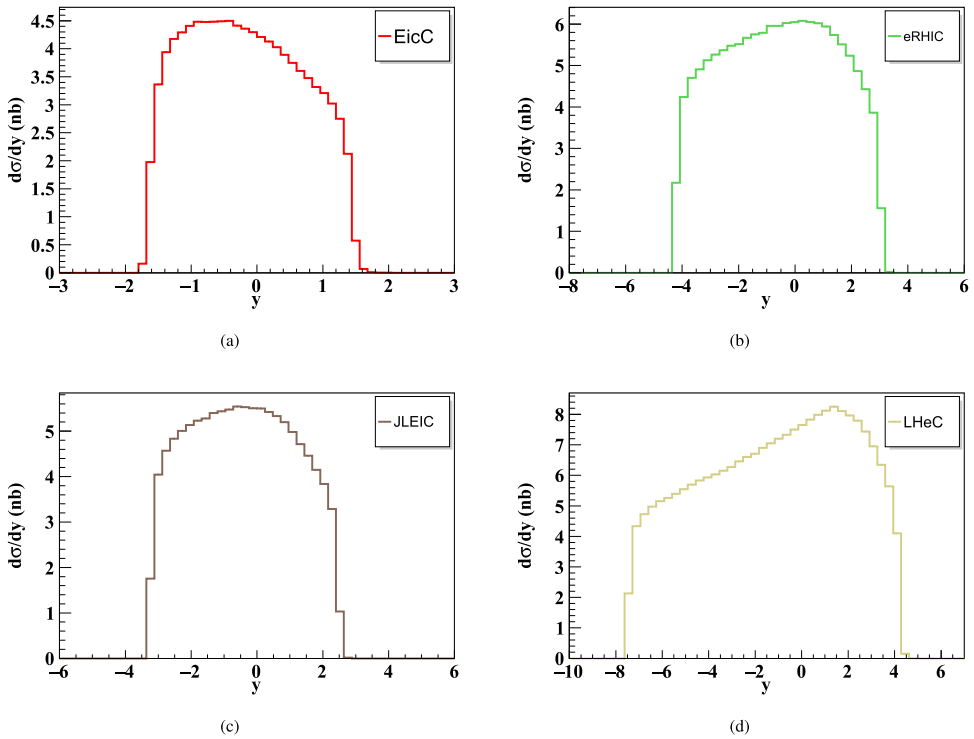

Fig. 8 The rapidity distribution of $\phi(1680)$ in EicC (**a**), eRHIC (**b**), JLEIC (**c**) and LHeC (**d**) at $0.10\ \text{GeV}^2 < Q^2 < 1.00\ \text{GeV}^2$

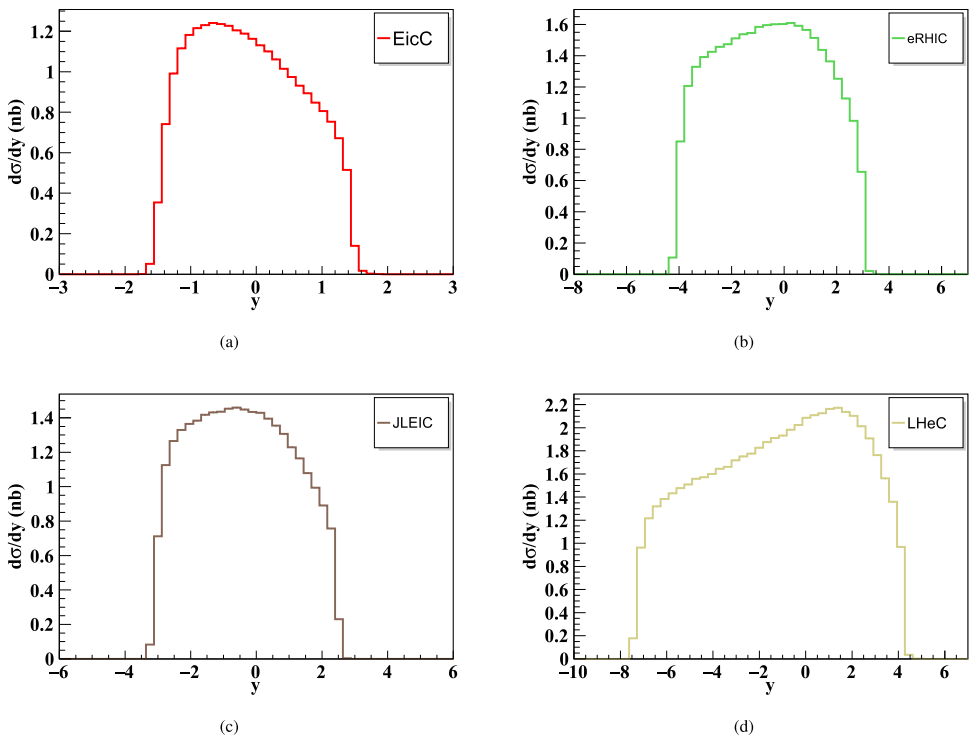

Fig. 9 The rapidity distribution of $\phi(1680)$ at EICs at $1.00\ \text{GeV}^2 < Q^2 < 5.00\ \text{GeV}^2$

tion is mostly concentrated in the middle part, and the events generated are sufficient. Moreover, the cross sections of production are enormous, and the rates are over 2 billion. These phenomena indicate that the $\phi(1680)$ may be detected by the LHC and RHIC. Investigating p–A scattering in UPCs can quickly measure accurate data of the cross sections of $\phi(1680)$ production. This may deliver a crucial procedure for further studying the physical properties of $\phi(1680)$.

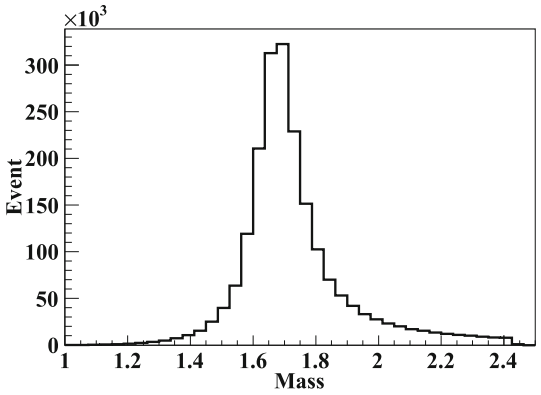

Fig. 10 The mass distribution of $\phi(1680)$ is simulated at EicC [23] by using eSTARlight code [27,28]

Table 5 Beam energy, production total cross section σ and event for RHIC [20] and LHC [21]

Accelerator	Beam	Energy (GeV)	σ (mb)	Event (B)
RHIC	p/Au	100/100	0.524 mb	2.358
LHC	p/Pb	7000/2778	3.525 mb	7.100

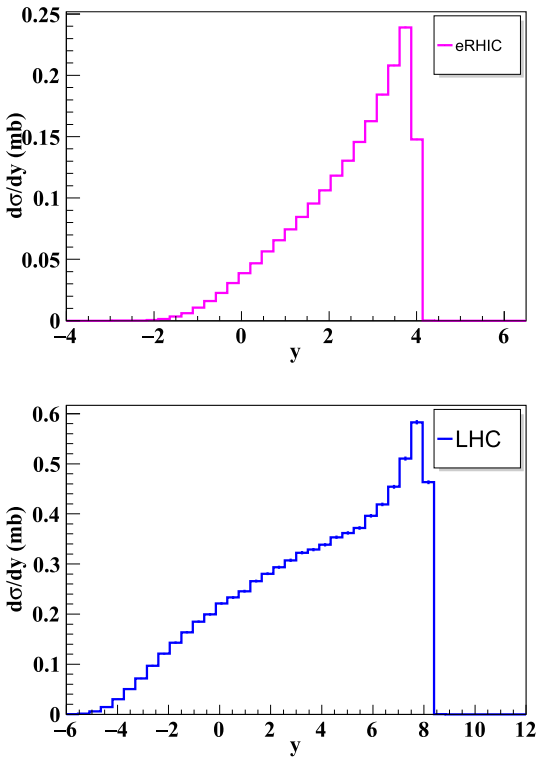

Fig. 11 The rapidity distribution of $\phi(1680)$ at eRHIC (top) and LHC (bottom)

4 Conclusion

In this work, based on the photoproduction of $\phi(1020)$ [17], we predict the total and differential cross sections of $\phi(1680)$ photoproduction at the near-threshold by the two gluon exchange model and the pomeron model. The predicted cross section size is about 1/5 of $\phi(1020)$. Further, under the guidance of VMD model, the RMS of scattering length of $\phi(1680)$-p interaction is calculated as $|\alpha_{\phi(1680)p}| = 0.07 \pm 0.01$ fm. This result deviates from the $\alpha_{Vp} \propto \exp(1/m_V)$, which is a little bit different than what we concluded before [53]. Considering that $\phi(1680)$ is the first excited state of $\phi(1020)$ and both are $s\bar{s}$ state structure, it is reasonable that the scattering length is close.

Furthermore, we use two existing programs to calculate the total production cross section, event rates and rapidity distribution of $\phi(1680)$ at four EICs and two UPCs. For the e–p scattering at EICs, the production rates are predicted to exceed 100 million events per year at different Q^2 intervals. At such a production rate, it is possible to observe a wide range of W^2 and Q^2 electroproduction in an acceptable detector. Meanwhile, the p–A scattering at UPCs also have opportunities to detect the production of $\phi(1680)$. This is an excellent chance for future research on the properties of this state.

In order to comprehensively study the physical characteristics of $\phi(1680)$, a considerable number of the cross sectional data of $\gamma p \to \phi(1680)p$ are required, and the most meaningful data is the result near the threshold. Future United States EIC [22] and the EicC [23] will provide a significant opportunity to probe these cross sections. In addition, the GlueX laboratory [51] at Jefferson Lab intends to conduct photoproduction experiments on a LH_2 target for strangeness states. At the same time, the CLAS12 detector [52] will also provide a world-leading facility to explore strangeness states through e–p scattering experiments. These experiments will produce abundant data for in-depth study in the future.

Acknowledgements This work is supported by the National Natural Science Foundation of China under Grants no. 12065014 and no. 12047501, and by the Natural Science Foundation of Gansu province under Grant no. 22JR5RA266. We acknowledge the West Light Foundation of The Chinese Academy of Sciences, Grant no. 21JR7RA201.

Data Availability Statement This manuscript has no associated data or the data will not be deposited. [Authors' comment: All the relevant data are already contained in the manuscript.]

Open Access This article is licensed under a Creative Commons Attribution 4.0 International License, which permits use, sharing, adaptation, distribution and reproduction in any medium or format, as long as you give appropriate credit to the original author(s) and the source, provide a link to the Creative Commons licence, and indicate if changes were made. The images or other third party material in this article are included in the article's Creative Commons licence, unless indicated otherwise in a credit line to the material. If material is not included in the article's Creative Commons licence and your intended use is not permitted by statutory regulation or exceeds the permitted use, you will need to obtain permission directly from the copyright holder. To view a copy of this licence, visit http://creativecommons.org/licenses/by/4.0/.

Funded by SCOAP[3]. SCOAP[3] supports the goals of the International Year of Basic Sciences for Sustainable Development.

References

1. Q. Li, L.C. Gui, M.S. Liu, Q.F. Lü, X.H. Zhong, Mass spectrum and strong decays of strangeonium in a constituent quark model. Chin. Phys. C **45**, 023116 (2021)
2. P.L. Liu, S.S. Fang, X.C. Lou, Strange quarkonium states at BESIII. Chin. Phys. C **39**, 082001 (2015)
3. S. Godfrey, N. Isgur, Mesons in a relativized quark model with chromodynamics. Phys. Rev. D **32**, 189–231 (1985)
4. T. Barnes, N. Black, P.R. Page, Strong decays of strange quarkonia. Phys. Rev. D **68**, 054014 (2003)
5. P.A. Zyla et al. (Particle Data Group), Review of particle physics. PTEP **2020**, 083C01 (2020)
6. V.E. Barnes, D. Bassano, S.U. Chung, R.L. Eisner, E. Flaminio, J.B. Kinson, N.P. Samios, Production of p pi+ pi- enhancements from the reaction $k^- p -> p\pi + \pi^-$ at 3.9, 4.6, and 7.3 Gev/c. Phys. Rev. Lett. **23**, 1516–1520 (1969)
7. J.A. Danysz, B.R. French, V. Simak, Annihilations of 3.0 and 3.6 GeV/c antiprotons into six or more pions. Nuovo Cim. A **51**, 801 (1967)
8. J.A.J. Matthews, J.D. Prentice, T.S. Yoon, J.T. Carroll, M.W. Firebaugh, W.D. Walker, Production and decay of the $\phi(1680)$ in $\pi d \to pp\pi\pi\pi^0$ at 6.95 GeV/c. Phys. Rev. D **3**, 2561–2572 (1971)
9. F. Mane, D. Bisello, J.C. Bizot, J. Buon, A. Cordier, B. Delcourt, Study of $e^+e^- \to K_S^0 K^\pm \pi^\mp$ in the 1.4-GeV to 2.18-GeV energy range: a new observation of an isoscalar vector meson ϕ' (1.65-GeV). Phys. Lett. B **112**, 178–182 (1982)
10. J. Buon, D. Bisello, J.C. Bizot, A. Cordier, B. Delcourt, F. Mane, J. Layssac, Interpretation of Dm1 results on e^+e^- annihilation into exclusive channels between 1.4-GeV and 1.9-GeV with a $\rho'\omega'\phi'$ model. Phys. Lett. B **118**, 221 (1982)
11. D. Bisello et al. (DM2), Study of the reaction $e^+e^- \to K^+K^-$ in the energy range $1350 \leq \sqrt{s} \leq 2400$-MeV. Z. Phys. C **39**, 13 (1988)
12. R.R. Akhmetshin, V.M. Aulchenko, V.S. Banzarov, L.M. Barkov, S.E. Baru, N.S. Bashtovoy, A.E. Bondar, D.V. Bondarev, A.V. Bragin, S.K. Dhawan et al., Study of the process $e^+e^- \to K^0(L)K^0(S)$ in the CM energy range 1.05-GeV to 1.38-GeV with CMD-2. Phys. Lett. B **551**, 27–34 (2003)
13. C.Q. Pang, Excited states of ϕ meson. Phys. Rev. D **99**, 074015 (2019)
14. J.N. de Quadros, D.T. Da Silva, M.L.L. Da Silva, D. Hadjimichef, Strong decays of strange quarkonia in a corrected $^3P_0$ model. Phys. Rev. C **101**, 025203 (2020)
15. B. Aubert et al. (BaBar), Measurements of $e^+e^- \to K^+K^-\eta$, $K^+K^-\pi^0$ and $K_s^0 K^\pm\pi^\mp$ cross-sections using initial state radiation events. Phys. Rev. D **77**, 092002 (2008)
16. K.A. Olive et al. (Particle Data Group), Review of particle physics. Chin. Phys. C **38**, 090001 (2014)
17. X.Y. Wang, C. Dong, Q. Wang, Mass radius and mechanical properties of the proton via strange ϕ meson photoproduction. Phys. Rev. D **106**, 056027 (2022)
18. C.A. Bertulani, S.R. Klein, J. Nystrand, Physics of ultra-peripheral nuclear collisions. Annu. Rev. Nucl. Part. Sci. **55**, 271–310 (2005)
19. M. Strikman, Perspectives of probing small-x dynamics in protons and nuclei in ultraperipheral A A and p A collisions at LHC. Nucl. Phys. B Proc. Suppl. **179–180**, 111–116 (2008)
20. M. Tanabashi et al. (Particle Data Group), Review of particle physics. Phys. Rev. D **98**, 030001 (2018)
21. Z. Citron, A. Dainese, J.F. Grosse-Oetringhaus, J.M. Jowett, Y.J. Lee, U.A. Wiedemann, M. Winn, A. Andronic, F. Bellini, E. Bruna et al., Report from Working Group 5: future physics opportunities for high-density QCD at the LHC with heavy-ion and proton beams. CERN Yellow Rep. Monogr. **7**, 1159–1410 (2019)
22. A. Accardi, J.L. Albacete, M. Anselmino, N. Armesto, E.C. Aschenauer, A. Bacchetta, D. Boer, W.K. Brooks, T. Burton, N.B. Chang et al., Electron ion collider: the next QCD frontier: understanding the glue that binds us all. Eur. Phys. J. A **52**, 268 (2016)
23. D.P. Anderle, V. Bertone, X. Cao, L. Chang, N. Chang, G. Chen, X. Chen, Z. Chen, Z. Cui, L. Dai et al., Electron-ion collider in China. Front. Phys. (Beijing) **16**, 64701 (2021)
24. V. Morozov, in *Presented at the EIC Users Group Meeting, 2017* (Trieste, Italy, 2017)
25. J.L. Abelleira Fernandez et al. (LHeC Study Group), A large hadron electron collider at CERN: report on the physics and design concepts for machine and detector. J. Phys. G **39**, 075001 (2012)
26. S.R. Klein, J. Nystrand, J. Seger, Y. Gorbunov, J. Butterworth, STARlight: a Monte Carlo simulation program for ultra-peripheral collisions of relativistic ions. Comput. Phys. Commun. **212**, 258–268 (2017)
27. M. Lomnitz, S. Klein, Exclusive vector meson production at an electron-ion collider. Phys. Rev. C **99**, 015203 (2019)
28. M. Lomnitz, Coherent vector meson production at an electron ion collider. PoS **DIS2018**, 171 (2018)
29. Y.P. Xie, X.Y. Wang, X. Chen, Probing charmonium-like XYZ states in hadron–hadron ultraperipheral collisions and electron–proton scattering. Eur. Phys. J. C **81**, 710 (2021)
30. X.Y. Wang, W. Kou, Q.Y. Lin, Y.P. Xie, X. Chen, A. Guskov, Production of the bottomonium-like states Z_b states at e-h and ultra-peripheral h-h collisions. Chin. Phys. C **45**, 5 (2021)
31. Y.P. Xie, V.P. Goncalves, Probing hidden-bottom pentaquarks in fixed-target collisions at the LHC. Phys. Lett. B **814**, 136121 (2021)
32. A.I. Titov, T. Nakano, S. Date, Y. Ohashi, Comments on differential cross-section of phi-meson photoproduction at threshold. Phys. Rev. C **76**, 048202 (2007)
33. L. Pentchev, I.I. Strakovsky, J/ψ-p scattering length from the total and differential photoproduction cross sections. Eur. Phys. J. A **57**, 56 (2021)
34. I. Strakovsky, D. Epifanov, L. Pentchev, J/ψp scattering length from GlueX threshold measurements. Phys. Rev. C **101**, 042201 (2020)
35. I.I. Strakovsky, L. Pentchev, A. Titov, Comparative analysis of ωp, ϕp, and $J/\psi p$ scattering lengths from A2, CLAS, and GlueX threshold measurements. Phys. Rev. C **101**, 045201 (2020)
36. A.M. Badalian, B.L.G. Bakker, The Regge trajectories and leptonic widths of the vector $s\bar{s}$ mesons. Few Body Syst. **60**, 58 (2019)
37. F. Zeng, X.Y. Wang, L. Zhang, Y.P. Xie, R. Wang, X. Chen, Near-threshold photoproduction of J/ψ in two-gluon exchange model. Eur. Phys. J. C **80**, 1027 (2020)
38. M.E. Peskin, D.V. Schroeder, *An Introduction to Quantum Field Theory* (Addison-Wesley, Boston, 1995), p. 842
39. J.M. Laget, R. Mendez-Galain, Exclusive photoproduction and electroproduction of vector mesons at large momentum transfer. Nucl. Phys. A **581**, 397–428 (1995)
40. A. Sibirtsev, S. Krewald, A.W. Thomas, Systematic analysis of charmonium photoproduction. J. Phys. G **30**, 1427–1444 (2004)
41. P.V. Landshoff, Nonperturbative effects at small x. Nucl. Phys. B Proc. Suppl. **18**, 211–219 (1991)
42. S.V. Goloskokov, Electroproduction of light vector mesons. arXiv:0712.3968 [hep-ph]
43. M. Glück, E. Reya, A. Vogt, Dynamical parton distributions revisited. Eur. Phys. J. C **5**, 461–470 (1998)
44. R.D. Ball et al. (NNPDF), Unbiased global determination of parton distributions and their uncertainties at NNLO and at LO. Nucl. Phys. B **855**, 153–221 (2012)

45. J.F. Owens, A. Accardi, W. Melnitchouk, Global parton distributions with nuclear and finite-Q^2 corrections. Phys. Rev. D **87**, 094012 (2013)
46. A. Accardi, L.T. Brady, W. Melnitchouk, J.F. Owens, N. Sato, Constraints on large-x parton distributions from new weak boson production and deep-inelastic scattering data. Phys. Rev. D **93**, 114017 (2016)
47. J. Pumplin, D.R. Stump, J. Huston, H.L. Lai, P.M. Nadolsky, W.K. Tung, New generation of parton distributions with uncertainties from global QCD analysis. JHEP **07**, 012 (2002)
48. S.R. Klein, Y.P. Xie, Photoproduction of charged final states in ultraperipheral collisions and electroproduction at an electron-ion collider. Phys. Rev. C **100**, 024620 (2019)
49. V.M. Budnev, I.F. Ginzburg, G.V. Meledin, V.G. Serbo, The two photon particle production mechanism. Physical problems. Applications. Equivalent photon approximation. Phys. Rep. **15**, 181–281 (1975)
50. S. Klein, J. Nystrand, Exclusive vector meson production in relativistic heavy ion collisions. Phys. Rev. C **60**, 014903 (1999)
51. P. Pauli (GlueX), The strangeness program at GlueX. EPJ Web Conf. **271**, 02001 (2022)
52. G. Angelini (CLAS and CLAS12 RICH), CLAS12 RICH: new hybrid geometry for strangeness studies. Few Body Syst. **59**(6), 122 (2018). https://doi.org/10.1007/s00601-018-1443-2
53. X.Y. Wang, C. Dong, Q. Wang, Analysis of the interaction between of ϕ meson and nucleus. Chin. Phys. C **47**, 014106 (2023)
54. X.Y. Wang, F. Zeng, Q. Wang, L. Zhang, First extraction of proton mass radius and scattering length $\left|\alpha_{\rho^0 p}\right|$ from ρ^0 photoproduction. Sci. China Phys. Mech. Astron. **66**, 232012 (2023)
55. X.Y. Wang, F. Zeng, I.I. Strakovsky, The $\psi^{(*)} p$ scattering length based on near-threshold charmoniums photoproduction. Phys. Rev. C **106**, 015202 (2022)
56. I.I. Strakovsky, S. Prakhov, Y.I. Azimov, P. Aguar-Bartolomé, J.R.M. Annand, H.J. Arends, K. Bantawa, R. Beck, V. Bekrenev, H. Berghäuser et al., Photoproduction of the ω meson on the proton near threshold. Phys. Rev. C **91**, 045207 (2015)
57. I.I. Strakovsky, W.J. Briscoe, L. Pentchev, A. Schmidt, Threshold Upsilon-meson photoproduction at the EIC and EicC. Phys. Rev. D **104**, 074028 (2021)
58. W.C. Chang, K. Horie, S. Shimizu, M. Miyabe, D.S. Ahn, J.K. Ahn, H. Akimune, Y. Asano, S. Date, H. Ejiri et al., Forward coherent phi-meson photoproduction from deuterons near threshold. Phys. Lett. B **658**, 209–215 (2008)